Ion−Solvent Interactions in Acetonitrile Solutions of Lithium, Sodium, and Tetraethylammonium Perchlorate Using Attenuated Total Reflectance FTIR Spectroscopy

John S. Loring and W. Ronald Fawcett*

Department of Chemistry, University of California, Davis, California 95616

Received: December 4, 1998; In Final Form: February 24, 1999

A vibrational spectroscopic study of ion solvation in LiClO₄−, NaClO₄−, and tetraethylammonium perchlorate− acetonitrile solutions has been performed using attenuated total reflection FTIR spectroscopy. Spectra were curve fitted in the C≡N stretching and C−C≡N bending regions of the solvent using a multiple-dimensional fitting routine that factors an entire set of solution spectra into their physically real basis spectra according to a user supplied mathematical model. The spectra of the solutions of tetraethylammonium perchlorate in acetonitrile were shown to be a linear combination of one physically real basis spectrum that accounts for self-associated acetonitrile and another that accounts for the spectrum of the acetonitrile molecules associated with the perchlorate anion. It is demonstrated for the first time that the C≡N stretching band of acetonitrile molecules associated with ClO₄⁻ anions has a significantly different molar absorption coefficient from the same band for self-associated acetonitrile. The spectra of LiClO4 and NaClO4 solutions in acetonitrile were shown to be a linear combination of one physically real basis spectrum that accounts for the spectrum of self-associated acetonitrile and another that accounts for the spectrum of the acetonitrile molecules associated with both the cation and the anion. The fractional contribution of these physically real basis spectra to the solution spectra depends on the total electrolyte concentration, rather than on the extent of ion pairing. Two possible rationalizations for this phenomenon are discussed.

Introduction

Vibrational spectroscopy has been used effectively to study aprotic electrolyte solution structure and dynamics.[1−3] The analysis of acetonitrile(ACN)−electrolyte systems via a vibrational spectroscopic approach has been justified by the following: (1) the vibrational spectrum of pure ACN is well characterized and relatively simple, containing several sharp and well-separated bands; (2) for ACN−electrolyte solutions, many vibrational bands are readily distinguished that are due to ACN molecules associated with ions; (3) the vibrational bands of polyatomic anions of most inorganic salts that are soluble in ACN do not overlap significantly with the solvent bands. For these reasons, vibrational spectroscopy has been applied repeatedly to investigations of ion solvation and ion pairing in ACN− electrolyte solutions.[4−16]

The intermolecular structure of pure ACN consists primarily of molecules that are self-associated in antiparallel configurations, as confirmed by recent X-ray diffraction studies and reverse Monte Carlo simulations.[17−19] In ACN−electrolyte solutions, it has been assumed here that ACN molecules not influenced by the presence of ions or ion pairs have the same self-associated structure as pure ACN, as well as the same vibrational spectrum. With the addition of electrolyte and the increase in its concentration, new vibrational bands appear and grow in absorbance that are blue shifted from the positions of the self-associated ACN C≡N stretch (ν_2), C−C≡N bend overtone ($2\nu_8$), and CH₃ symmetric deformation + C−C stretch combination band ($\nu_3 + \nu_4$). These new bands have been assigned to ACN molecules that solvate cations, since the magnitudes of their shifts are independent of the anion present and scale with the charge-to-radius ratio of the cation.[14,20] The

shift of these cation-solvating ACN bands to higher wavenumbers is explained by the partial C≡N and C−C antibonding character of the molecular orbital that encompasses most of the lone pair electrons on the nitrogen. Thus, the transfer of the electron density in this molecular orbital to a cation leads to greater bond strengths in the associated vibrational modes.[21]

Cation solvation numbers for ACN−electrolyte solutions have been calculated in previous studies, based on one of two analytical approaches. Both methods utilize only the ACN ν_2 spectral region and rely on the assumption that the ν_2 band of ACN molecules influenced by anions is indistinguishable from the ν_2 band of self-associated ACN. The approaches differ with respect to their assumptions regarding ion pairing and its effect on the solution spectrum. In previous studies from this laboratory,[12−14] it was assumed that an anion in an ion pair displaces some, but not all, ACN molecules from the first solvation sphere of the cation, and that the ν_2 band of ACN molecules associated with ion-paired cations is indistinguishable from the ν_2 band of ACN molecules that are interacting with free cations. These assumptions, together with the total concentration of ACN and the integrated absorbance of the self- and anion-associated ACN ν_2 band, allowed the calculation of the concentration of ACN that interacts with both ion-paired and free cations. An average cation solvation number was estimated by dividing the concentration of ACN that interacts with ion-paired and free cations by the concentration of the electrolyte. In the second approach, used by Perelygin,[7] a curve fit was performed on solution spectra obtained at several different electrolyte concentrations in the absorption region of the electrolyte's polyatomic anion, and the bands due to ion-paired and free anions were separated. Ion paired cations were assumed not to be solvated, and a decrease in the integrated absorbance of the ν_2 band of self- and anion-associated ACN

Ion−Solvent Interactions in Acetonitrile Solutions

J. Phys. Chem. A, Vol. 103, No. 19, 1999 **3609**

was assumed to result from an increase in the concentration of ACN molecules solvating free cations. The concentrations of the electrolyte, the integrated absorbances of the ion-paired anion bands, and the integrated absorbance of the self- and anion-associated ν_2 band of ACN were then used in a simultaneous determination of the cation solvation number and the molar absorption coefficients of the bands due to the ion-paired anion.[7] Barthel[15] recently extended Perelygin's method by assuming that both contact and solvent-separated ion pairs exist simultaneously in solution and can be distinguished spectroscopically, that no ACN molecules are associated with or influenced by cations in contact ion pairs, and that the ν_2 band of ACN molecules in solvent-separated ion pairs is indistinguishable from the ν_2 band of ACN molecules that are interacting with free cations. These assumptions allowed the simultaneous determination of the combined solvation number for cations that are both free and in solvent-separated ion pairs, as well as the molar absorption coefficients of the contact-ion-paired anion bands.[15]

In the present paper, ion solvation in the LiClO₄− and NaClO₄−ACN systems is reinvestigated. Furthermore, the tetraethylammonium perchlorate (TEAP) system in ACN is examined in order to assess the role of the anion more carefully. Evidence is presented that conflicts with some of the basic assumptions made in previous vibrational spectral analyses of the alkali-perchlorate−ACN systems studied here.[4,7,13,15] Solution spectra were collected using attenuated total reflection (ATR) Fourier transform infrared (FTIR) spectroscopy. Moreover, the ATR spectra were converted to linear napierian absorption coefficient spectra using the method of Bertie,[22,23] essentially correcting for distortions in ATR spectra that result from variations in the real part of the solution refractive index with wavenumber and solution composition.[24] Two types of curve fitting were used. Single-dimensional spectral fits were performed, using a program that allows the linking of parameters that are theoretically not linearly independent.[25] For example, this program can force the integrated areas of peaks fitted to two bands arising from the same species in solution to be related by the known ratio of their molar absorption coefficients. The linking of parameters allows for considerably more user control over the curve fitting process. In addition, multiple-dimensional spectral fits were carried out, using a program capable of curve fitting an entire set of related spectra by utilizing the changes which take place in common spectral features from one spectrum to the next.[26] Multiple-dimensional curve fitting is significantly more powerful than single-dimensional fitting. The curve fitting techniques used are explained in detail in the Methods section.

Methods

Solution Preparation. Anhydrous ACN (99.8%, <0.005% water) was obtained from Aldrich and was used without further purification. LiClO₄ (Aldrich, 99.99%), NaClO₄ (Aldrich, 99%), and TEAP (GFS Chemicals) were dried under vacuum at 140 °C until the pressure in the drying pistol dropped to 1×10^{-4} Torr. The ACN and the drying pistols with salts were first opened in a glovebox filled with dry nitrogen, and all subsequent solution preparation was performed under water-free conditions. All solutions were prepared by weight. The concentration of each solution was calculated on the mole fraction concentration scale, but was later converted to molarity by use of an independent measurement of solution densities.

For each type of electrolyte solution, a series of density measurements was performed using a 20 mL tube pycnometer at 25 °C. Densities were collected at six equally spaced mole

fraction concentrations, ranging from pure ACN to the highest electrolyte concentration analyzed by vibrational spectroscopy. A second-degree polynomial with an intercept relating solution density to solution mole fraction was calculated, and this polynomial was used in the conversion from mole fraction to molarity for those solutions analyzed spectroscopically. The propagated standard deviation of the calculated solution molarities was better than ±0.006 M.

Concentrations of the electrolyte solutions studied ranged from pure ACN to 0.923, 1.032, and 0.680 M for LiClO₄, NaClO₄, and TEAP ACN solutions, respectively.

ATR Spectra Collection. A custom-built overhead ATR cell with a 45° and 50 × 20 × 3 mm trapezoidal cadmium telluride internal reflection element and a Teflon boat was mounted in a Mattson Galaxy 3000 FTIR spectrometer. The FTIR spectrometer was purged with dry nitrogen and was equipped with a Ge/KBr beam splitter, an air-cooled globar source, and a DTGS detector. Each single-beam mid-IR spectrum resulted from a 128 interferogram average that was Fourier transformed using boxcar apodization. All spectra were obtained between 4000 and 400 cm⁻¹, using 1 cm⁻¹ resolution. ATR spectra were calculated by taking the negative decadic logarithm of the ratio of sample and background single-beam spectra. The empty ATR cell blanketed with dry nitrogen was used to collect the background single-beam spectrum.

ATR Spectra to Linear Absorption Coefficient Spectra Conversion. The effective path length of the evanescent wave in attenuated total reflection, which is analogous to the path length in a conventional transmission experiment, has a dependence on the wavelength of the light and on the real part of the imaginary refractive index of the solution being analyzed. These dependencies result in two types of distortions in an ATR spectrum.[24] (1) The longer the wavelength of the light, the larger is the effective path length. Therefore, on comparison of an ATR spectrum to an absorbance spectrum collected in a constant path length transmission experiment, it is obvious that in the ATR spectrum the vibrational bands at higher wavenumbers (shorter wavelengths) are significantly smaller in size, relative to bands at lower wavenumbers (longer wavelengths). (2) The more closely matched are the real refractive indices of the solution and internal reflection element, the larger is the effective path length. Since the real refractive index changes considerably around the position of an absorption band, bands in ATR spectra are often slightly shifted and more asymmetric than the corresponding bands in an absorbance spectrum collected in a constant path length transmission experiment.

The effective path length's dependence on the real refractive index can cause significant errors in the quantitative analysis of ATR spectra. The magnitude of the change in the real refractive index is larger for bands of greater absorbances, resulting from a large molar absorption coefficient or due to the presence of a high concentration of a solution species. Consequently, as a vibrational band grows in absorbance with increased species concentration, the distortion in that band, as well as adjacent overlapping bands of completely different species, worsens to the degree that their shapes, positions, and heights are significantly altered. Without proper data treatment to correct for these distortions, significant errors in curve fitting arise.[24]

By converting ATR spectra to linear napierian absorption coefficient spectra, distortions due to changes in effective path length are removed. To perform this ATR spectrum conversion, a program called Spectral Conversion Tool[27] was written which utilizes the method of Bertie,[22,23] an iterative procedure based

on the Fresnel equations and the Kramers−Kronig transform. The only change to this method was the specification of the instrument index of polarization, determined with the use of a polarizer to be 0.43.

Calibration of the ATR cell was accomplished using a procedure similar to the methods used by Sperline[28] and Bertie.[29] The ATR spectrum of an optical standard (benzene) for which the infrared refractive indices are tabulated was collected with both s- and p-polarized light. Then, initial guesses were made for the angle of incidence and the number of reflections. The true values of these parameters were determined through a minimization of the sum of the squares of the deviations between the calculated and measured s- and p-polarized ATR spectra. The number of reflections and the angle of incidence were determined to be 6.2 and 49.4°, respectively. The anchor point (n_∞) used in the linear absorption coefficient spectrum calculation for all ACN-electrolyte solutions was approximated as the real refractive index at the sodium D line of pure ACN at 20 °C ($n_D = 1.3330$).[30]

Single-Dimensional Spectral Curve Fits. LinkFit[25] was used to perform single-dimensional spectral curve fits. The program fits Lorentzian, Gaussian, or mixed Lorentzian−Gaussian curves to spectral bands via the Levenberg−Marquardt algorithm. Polynomial baselines can also be fit during the nonlinear least squares iteration, or they can be solved for and subtracted away prior to the curvefit.

LinkFit allows pairs of adjustable parameter types (peak centers, widths, heights, and mixed Lorentzian−Gaussian character) to be linked so that they are forced to have the same value, or to differ by a constant user-defined factor or increment. It is typical to link the heights of two peaks used to fit bands arising from the same species by a factor corresponding to a ratio of the molar absorption coefficients of those bands. In addition, the centers of two peaks can be forced to be separated by a fixed increment, the spacing between two peaks can be linked by a factor of the spacing between two others, the widths of two peaks can be forced to the same value, and the percentages Lorentzian−Gaussian character of two peaks can be linked. Adjustable parameters can also be fixed, or not allowed to vary from a user-defined value. Fixing a parameter or linking together two parameters removes a degree of freedom from the nonlinear least squares routine, thereby further constraining the fit. The progress of a curve fit is evaluated visually by observing the residual spectrum and numerically by using the sum of the squares of the deviations between the calculated and measured spectra.

Multiple-Dimensional Spectral Curve Fits. A multiple-dimensional spectral curve fit is best explained through the use of an idealized illustration.[31] Consider 10 spectra of solutions containing three different noninteracting species. Each of the 10 spectra (the raw data spectra) is a linear combination of the individual species spectra (the physically real basis spectra). The raw data spectra can be organized into a matrix **A** (the raw data matrix) so that the columns represent the individual raw data spectra and the rows are the linear absorption coefficients at the user-chosen wavenumbers. This matrix could be factored directly into two other matrixes, **A** = **BP**, where the three columns of **B** are the physically real basis spectra comprising the raw data spectra in **A**, and each of the 10 rows of **P** give the contributions of the physically real basis spectra to the corresponding individual raw data spectrum. The goals of a multiple-dimensional spectral curve fit are to determine the number of physically real basis spectra, calculate these physi-

cally real basis spectra, and determine the contribution of each physically real basis spectrum to each of the raw data spectra.

A multiple-dimensional spectral curve fit is simplified greatly by the utilization of a numerical analysis routine called a singular value decomposition (SVD). Because there are usually unknown parameters in the matrix **P** that are nonlinear with respect to **A**, a nonlinear least-squares algorithm is required to factor **A** into **B** and **P**. However, the direct factor analysis of **A** into **B** and **P** by nonlinear least squares is computationally inconvenient due to the large sizes of these matrixes. Since an SVD factors **A** into much smaller matrixes, it is more reasonable to transform this SVD output into **B** and **P** by nonlinear least squares.

Abstract basis spectra are calculated as a result of an SVD. These spectra usually do not have any physical meaning and are not all significant. Ideally, insignificant abstract basis spectra serve only to model the random noise contained in the raw data spectra. The significance of each abstract basis spectrum is indicated by the square of its corresponding singular value and by its observed spectral signal-to-noise. The number of significant abstract basis spectra is equivalent to the number of physically real basis spectra in **B**. This is, in fact, an important and advantageous result of the SVD algorithm, especially if there is no prior knowledge of the number of physically real basis spectra.

The program, SVD Spectral Analysis Tool,[26] was used to compute multiple-dimensional spectral curve fits. This program first performs an SVD on the raw data spectral matrix **A**. Then, it carries out a nonlinear least-squares fit of the SVD output to a user-supplied mathematical model (comprising the matrix **P**), using the Levenberg−Marquardt algorithm. The user-supplied mathematical model defines the composition of the raw data spectra in terms of the physically real basis spectra and as a function of known parameters that are characteristic of each raw data spectrum. SVD Spectral Analysis Tool computes the unknown parameters in the model, the physically real basis spectra in the matrix **B**, and the fractional contributions of the physically real basis spectra to each raw data spectrum in the matrix **P**.

Results and Discussion

Figure 1 shows vibrational spectra in the ν_2 and $2\nu_8$ spectral regions of ACN for 10 of the LiClO$_4$−ACN solutions studied. The ν_2, $2\nu_8$, and $\nu_3 + \nu_4$ bands of pure ACN are located at 2253, 750, and 2293 cm^{-1}, respectively. In LiClO$_4$−ACN solutions, bands due to ACN molecules solvating Li$^+$ grow in linear absorption coefficient with an increase in LiClO$_4$ concentration at approximately 2275, 773, and 2293 cm^{-1} for the ν_2, $2\nu_8$, and $\nu_3 + \nu_4$ bands, respectively. In the NaClO$_4$−ACN system, analogous bands grow in linear absorption coefficient with increasing NaClO$_4$ concentration at approximately 2265, 759, and 2298 cm^{-1}.

Single-Dimensional Curve Fits of the Spectra of LiClO$_4$ and NaClO$_4$−ACN Solutions. Single-dimensional curve fits of the ν_2 and $2\nu_8$ spectral regions of LiClO$_4$ and NaClO$_4$−ACN solutions were performed by applying the most basic assumption used previously,[7,8,12−15] namely, that self-associated ACN and ACN molecules influenced by ClO$_4$− have a vibrational spectrum identical to that of pure ACN. However, the number, types, and positions of the fitted bands used here differ from those used by previous authors.

The details of the curve fits that were conducted in the present study are as follows. The ν_2 band of pure ACN is asymmetric, containing a shoulder at lower wavenumbers. The source of this shoulder has been in dispute for some time. Some authors
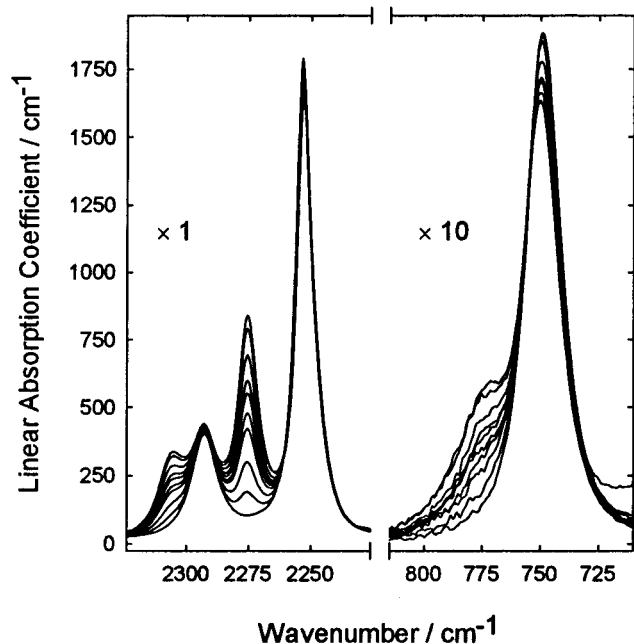
Ion−Solvent Interactions in Acetonitrile Solutions

J. Phys. Chem. A, Vol. 103, No. 19, 1999 **3611**

Figure 1. ACN ν_2 and $2\nu_8$ spectral regions of LiClO$_4$-ACN solutions of various concentrations, 0.000 (pure ACN), 0.098, 0.224, 0.368, 0.455, 0.538, 0.592, 0.723, 0.887, and 0.923 M, as proceeding from the lowest to the highest absorption coefficient of the ν_2 band of Li$^+$ solvating ACN, located at 2275 cm^{-1}.

Figure 2. Single-dimensional curve fit of the ν_2 and $2\nu_8$ spectral regions of pure ACN, as described in the text. The measured spectrum is indicated with a dashed line. The residual is offset for clarity.

contend that the shoulder is an intermolecular phenomenon and is due only to ACN molecules in a dimerized state,[32−35] while others assume that the shoulder is due to an intramolecular phenomenon and is caused by a series of hot bands.[15,36,37] The dimer explanation assumes that the structure of pure ACN is a mixture of both monomers and dimers, and the monomer is presumed to be the predominant species in the liquid. The shoulder is believed to be due to the ν_2 band of dimerized ACN that is red shifted from the significantly more intense ν_2 band of the ACN monomer.

The hot band explanation assumes that the ν_2 mode of ACN is strongly anharmonicly coupled to the C−C≡N bending mode (ν_8). Since the ν_8 mode is a low-energy vibration (fundamental at 378 cm^{-1}), then as much as 23% of the molecular population exists in the first excited state, 6% in the second, and nearly 2% is in the third excited state at room temperature, as predicted by the Boltzmann distribution. Furthermore, due to anharmonic coupling, the wavenumber position of the band arising from the ground state to first excited state transition of the ν_2 mode depends on the vibrational state of the ν_8 mode. Consequently, successive ν_2 hot bands (transitions for which the ν_8 mode is in an excited state) are offset from the ν_2 cold band (the transition for which the ν_8 mode is in the ground state) by a factor of the anharmonic coupling constant. The relative intensities of these bands are equivalent to the relative molecular populations in different the ν_8 mode vibrational states. Since an increase in temperature gives rise to increased molecular populations in ν_8 mode excited states and a decreased molecular population in the ν_8 ground state, the intensities of the ν_2 hot bands increase with temperature while that of the ν_2 cold band decreases.

The hot band explanation of the ν_2 band of ACN does not negate the existence of intermolecular associates. On the contrary, this explanation assumes that the cold band and each hot band pertains generally to self-associated ACN. However, the hot band explanation holds that it is not possible to distinguish between intermolecular associates of different associative strengths.
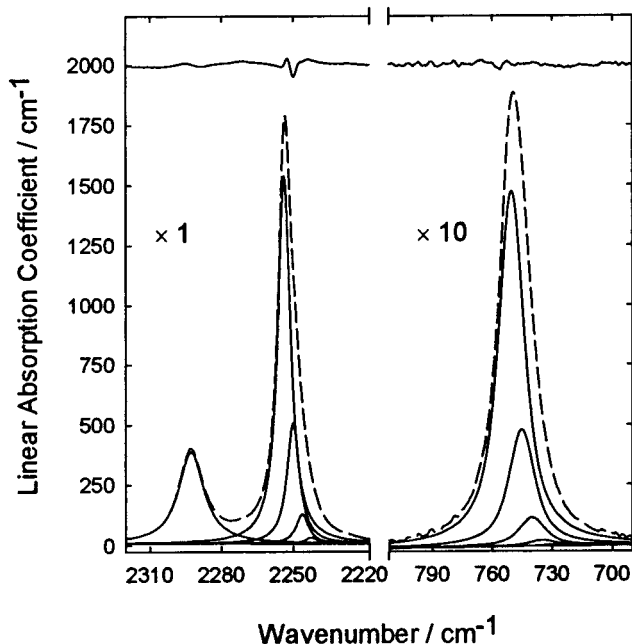
Consistent with the behavior of hot bands, the asymmetry of the ν_2 band of pure ACN increases with increasing temperature such that the shoulder protrudes to a greater degree at higher temperatures.[36] Accepting the hot band explanation for the ν_2 band asymmetry, the ν_2 band of pure ACN was curve fitted with a cold band and four hot bands, using the method of Hashimoto et al.,[37] as shown in Figure 2. Since the shape of vibrational bands of a molecule in the liquid state is governed primarily by intermolecular interactions, the mixed Lorentzian−Gaussian character and the widths of these bands were forced to be equal. The relative integrated areas of these bands were forced to match their theoretically predicted values from the Boltzmann distribution. Furthermore, the spacings between adjacent bands can be shown to equal the anharmonicity constant and were therefore constrained to coincide. This anharmonicity constant was calculated to be −3.8 cm^{-1}, which is comparable to the value in the gas phase, reported to be −4.9 cm^{-1}.[38]

Hot bands have been assigned to the $2\nu_8$ band of pure acetonitrile in the gas phase,[39] and it is reasonable to assume that this band will also contain hot bands in the liquid phase. To a first anharmonic approximation, it can be shown that the spacings between this overtone's cold band and hot bands are equal to 4 times the anharmonicity constant. Therefore, a cold band and four hot bands were fitted to this overtone in the same manner as explained above for the ν_2 band, as shown in Figure 2. The anharmonicity constant in the liquid was determined to be −5.2 cm^{-1}, whereas the gas-phase value has been reported to be −4.4 cm^{-1}.[39] However, it should be noted that since the C−C≡N bend is a doubly degenerate mode, in a higher and perhaps more appropriate anharmonic approximation, the cold and hot bands are each predicted to split further into two or more subbands.

Hot bands have also been assigned in gas-phase ACN for the $\nu_3 + \nu_4$ band.[38] However, since the spacing between the cold and hot bands in the gas phase was calculated to be less than a wavenumber, only a single band with mixed Lorentzian−Gaussian character was fitted to this combination band in the pure liquid.
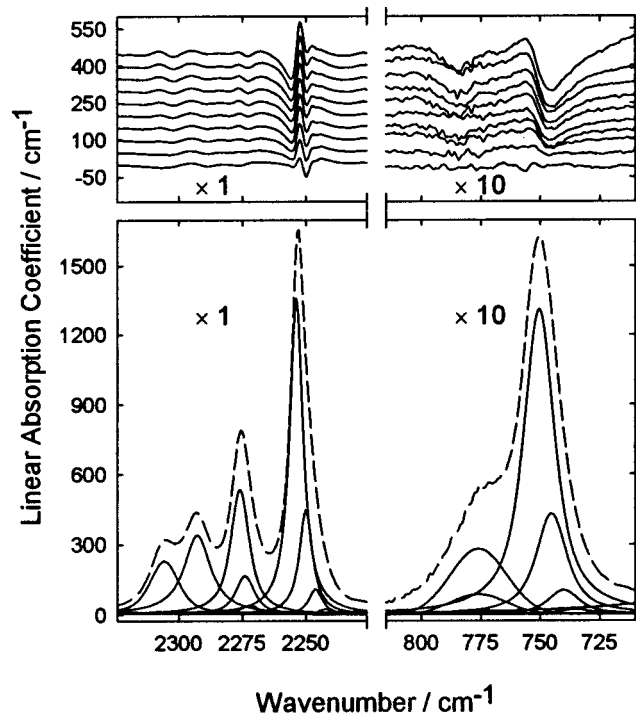
Figure 3. Single-dimensional curve fits of the ACN ν_2 and $2\nu_8$ spectral regions of LiClO$_4$−ACN solutions, as described in the text. (top) Residuals (offset for clarity) are shown for the curve fits of the spectra shown in Figure 1. The bottom-most residual is from the curve fit of the pure ACN spectrum, and each successive residual is from the curve fit of the spectrum of greater LiClO$_4$ concentration (concentrations given in Figure 1). (bottom) The curve fit of the 0.887 M LiClO$_4$−ACN solution spectrum. The measured spectrum is indicated with a dashed line.

The spectra of the LiClO$_4$ and NaClO$_4$−ACN solutions were curve fitted using the following method. The curve fits described above for the ν_2, $2\nu_8$, and $\nu_3 + \nu_4$ bands of pure ACN were assumed to be the correct fits of the corresponding bands of self- and ClO$_4^-$-associated ACN. Accordingly, all adjustable parameters of the self- and ClO$_4^-$-associated ACN bands were fixed, except for the peak heights. Furthermore, since the integrated areas of the self- and ClO$_4^-$-associated ACN bands are not linearly independent, the peak heights of these bands were linked by the ratios of their molar absorption coefficients. The spectrum of the solution with the highest concentration of electrolyte was used to determine the spectrum of the cation-solvating ACN. In the same manner as for the corresponding self- and ClO$_4^-$-associated ACN bands, the cation-solvating ACN ν_2 and $2\nu_8$ bands were each fitted with a cold band and four hot bands. Likewise, the $\nu_3 + \nu_4$ band of cation-solvating ACN was fitted with a single mixed Lorentzian−Gaussian curve. After the cation-solvating bands were determined using the spectrum obtained at the highest electrolyte solution concentration, the positions, widths, and mixed Lorentzian−Gaussian characters of these bands were fixed and their heights were linked by the ratios of their molar absorption coefficients. Then, the spectra of all other less concentrated electrolyte solutions were fitted under these constraints.

The curve fit of the ν_2 and $2\nu_8$ spectral regions for the solution with the highest concentration of LiClO$_4$ is shown in Figure 3. Included in this figure are the residuals resulting from this method of curve fitting of the 10 spectra shown in Figure 1. Figure 4 is a plot of the concentration of cation-solvating ACN versus the concentration of LiClO$_4$, based on this analysis. First,
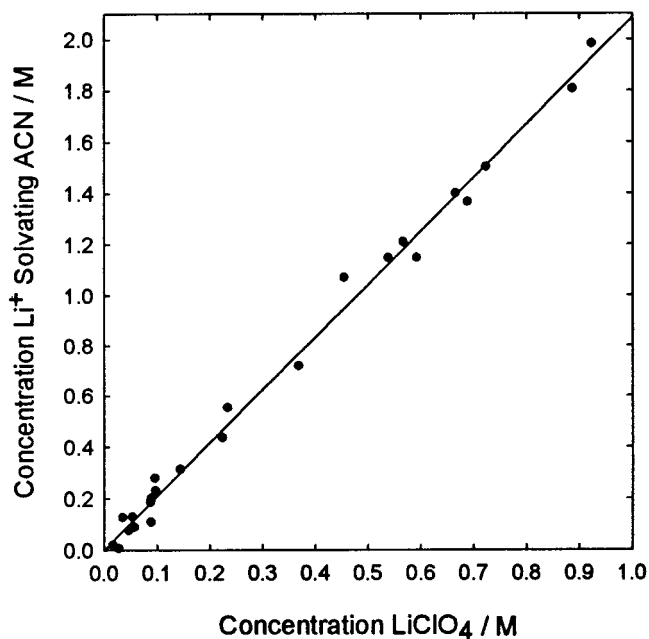

Figure 4. Concentration of Li$^+$-solvating ACN as a function of the concentration of LiClO$_4$ and based on the single-dimensional curve fit of the ACN ν_2 and $2\nu_8$ spectral regions of LiClO$_4$−ACN solutions, as described in the text. The slope of the fitted linear regression line is 2.08 ± 0.02.

the concentration of self- and ClO$_4^-$-associated ACN was calculated using the global integrated linear absorption coefficient of the self- and ClO$_4^-$-associated ACN bands, and using the global molar absorption coefficient of these bands determined from the spectrum of pure ACN. Then, the concentration of cation-solvating ACN was calculated by subtracting the concentration of self- and ClO$_4^-$-associated ACN from the total concentration of ACN in each solution. The slope of the linear regression line in Figure 4 (equaling 2.08 ± 0.02) can be defined as the average Li$^+$ solvation number.[12−14] Similar results were obtained when applying this method of curve fitting to the spectra of the NaClO$_4$−ACN solutions (average Na$^+$ solvation number equaling 1.86 ± 0.03).

The low value of the Li$^+$ and Na$^+$ average solvation numbers suggests either that there is extensive ion pairing or that the assumptions made in the single-dimensional fitting procedure described above are wrong. Both of these points have merit, and the latter deserves further attention, given that the residual spectrum of the 0.923 M LiClO$_4$−ACN solution accounts for as much as 4.7% of the integrated linear absorption coefficient of the measured spectrum, based on the spectral regions shown in Figure 3. From the positions of the minima and maxima of all the residuals in Figure 3, it is apparent that the problem with the single-dimensional curve fits lies primarily with the fits of the self- and ClO$_4^-$-associated ACN bands. One possibility that must be considered more carefully is that the strength of the ClO$_4^-$−ACN interaction is sufficient to alter the character of the ACN spectrum in the ν_2 and $2\nu_8$ spectral regions in a subtle but important way. This possibility is now explored in more detail.

Influence of ClO$_4^-$ on the ν_2 and $2\nu_8$ Spectral Regions of ACN. The results of the single-dimensional curve fits of the spectra of LiClO$_4$ and NaClO$_4$−ACN solutions seem to indicate that the spectrum of ClO$_4^-$-associated ACN is not identical to the spectrum of self-associated or pure ACN in the ν_2 and $2\nu_8$ spectral regions. To test this hypothesis, an analysis of the
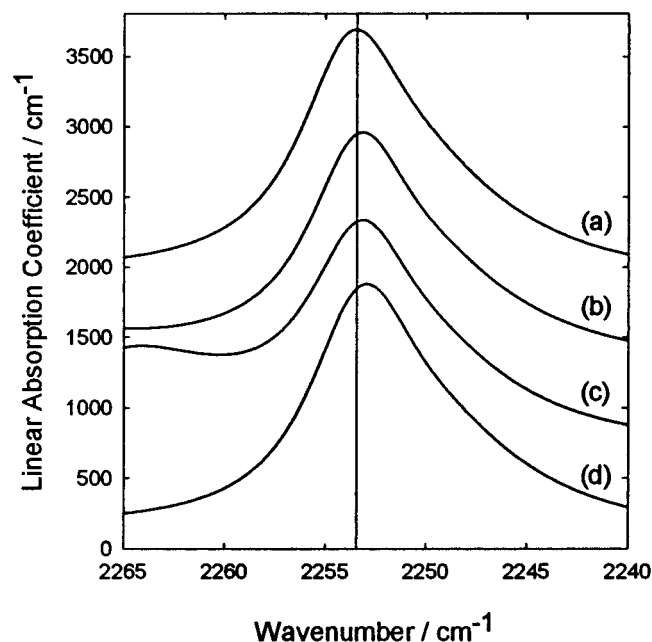
Ion−Solvent Interactions in Acetonitrile Solutions

J. Phys. Chem. A, Vol. 103, No. 19, 1999 **3613**

Figure 5. Coadded self- and ClO_4^--associated ACN ν_2 band from the spectra of pure ACN (a), a 0.923 M $LiClO_4$−ACN solution (b), a 1.032 M $NaClO_4$−CAN solution (c), and a 0.680 M TEAP−ACN solution (d).

spectra of solutions of TEAP in ACN was performed. Although the effects of ClO_4^- cannot be isolated from those of TEA^+ with complete confidence, the linear trend in the wavenumber shifts of the cation-solvating bands with charge-to-radius ratio[14,20] suggests that the shifts of the vibrational bands of ACN molecules interacting with TEA^+ should not be detectable. In the spectra of TEAP−ACN solutions, it is assumed here that ClO_4^- is the principal cause of the perturbations observed in the vibrational bands of the solvent.

The following evidence is cited, supporting the hypothesis that the spectrum of ACN molecules that are influenced by ClO_4^- is significantly different from that of self-associated ACN in the ν_2 and $2\nu_8$ spectral regions. Although the ν_2 band of pure ACN is centered at 2253.5 cm^{-1}, the maximum of the coadded self- and ClO_4^--associated ACN band consistently shifts 1 cm^{-1} to the red in the spectra of highly concentrated $LiClO_4$−, $NaClO_4$−, and TEAP−ACN solutions, as shown in Figure 5. This shift is noticeable in the spectra of the $NaClO_4$ and $LiClO_4$ solutions despite the overlap of the blue-shifted ν_2 band of cation-solvating ACN. The ClO_4^- anion, common to these electrolytes is the most likely cause of this slight red shift. The partial subtraction of the spectrum of pure ACN from the spectrum of a 0.680 M TEAP solution in the $2\nu_8$ spectral region leaves behind a band centered at roughly 754 cm^{-1}. It is not possible to completely subtract away this band, using the spectrum of pure ACN. In the spectra of the $LiClO_4$− and $NaClO_4$−ACN solutions, the partial subtraction of the spectrum of pure ACN not only leaves behind their respective $2\nu_8$ cation-solvating bands but also the anomalous band at approximately 754 cm^{-1}. Additionally, it is deduced from the partial subtraction of the pure ACN spectrum from the spectra of the less concentrated electrolyte solutions that the band at 754 cm^{-1} is growing in linear absorption coefficient with increasing electrolyte concentration. The source of this band is believed to be the $2\nu_8$ band of ACN influenced by ClO_4^-. Moreover, this subtraction also leaves a substantial ν_2 band centered at 2252.5 cm^{-1}, also believed to belong to ACN influenced by ClO_4^-. It

is important to add that the integrated linear absorption coefficient of the ν_2 band in spectra of TEAP−ACN solutions does not appear to decrease with an increase in TEAP concentration, although this electrolyte occupies a significant volume fraction of the solution. For example, the solution studied with the highest concentration of TEAP only has an ACN concentration of 16.87 M, compared to the 18.88 M concentration of pure ACN. Thus, a new ν_2 band having a significantly larger molar absorption coefficient than the ν_2 band of pure ACN must be growing in linear absorption coefficient with increase in TEAP concentration. This band is most likely arising from the ACN molecules influenced by ClO_4^-.

The strength of the interaction between ClO_4^- and ACN is debatable. ACN is considered a poor acceptor of electrons, having a Gutmann acceptor number of only 18.9,[40] and is generally not expected to associate with anions as an electron acceptor to the extent that it associates with cations as an electron donor. On the other hand, Perelygin has reported that the vibrational spectrum of ACN is significantly affected by the anion present. Semiempirical quantum mechanical calculations show that the lowest energy configuration of an anion− ACN complex is with the anion oriented along one of the C−H bonds on the methyl group.[41,42] Accordingly, SCN^- and I^- anions give rise to wavenumber shifts (of as much as 20 cm^{-1}) and increases in the molar absorption coefficients of the C−H stretching bands of ACN (ν_1 and ν_5).[21] While the ClO_4^- and NO_3^- anions do not give rise to detectable shifts in the ν_1 and ν_5 bands, these anions do cause increases in the bands' molar absorption coefficients.[4,7,13,21] For example, the percent increase in the integrated linear absorption coefficient in the ν_1 and ν_5 regions (from 2850 to 3100 cm^{-1}) between the pure ACN spectrum and the spectra of 0.887 M $LiClO_4$ and 0.881 M $NaClO_4$−ACN solutions is 21.9% and 22.3%, respectively. Furthermore, the calculated bond energy between an ACN molecule and ClO_4^- is 34 kJ mol^{-1}, compared to 173 kJ mol^{-1} of an ACN−Li^+ bond[41,42] and 24.8 kJ mol^{-1} of the calculated binding energy of an ACN antiparallel dimer.[43] These observations suggest that the strength of a ClO_4^- −ACN interaction might be comparable to that of cation solvation.

Multiple-Dimensional Curve Fits of the Spectra of TEAP, $LiClO_4$, and $NaClO_4$ Solutions. Since the ν_2 band of ClO_4^--associated ACN is only slightly red shifted from the ν_2 band of self-associated ACN, and since two bands of the TEA^+ cation (797 and 786 cm^{-1}) overlap with the $2\nu_8$ bands of self-associated and ClO_4^--associated ACN (750 cm^{-1} and approximately 754 cm^{-1}, respectively), single-dimensional curve fits of the ν_2 and $2\nu_8$ regions of the spectra of TEAP−ACN solutions have proved to be futile. However, a multiple-dimensional curve fit of these spectra is highly successful in elucidating the influence of the ClO_4^- anion on the spectrum of ACN, assuming a fixed number of ACN molecules influenced by ClO_4^-.

Six spectra of solutions ranging in concentration from pure ACN to 0.680 M TEAP were used to create the raw data matrix **A**. Not only were the ν_2 and $2\nu_8$ regions used for this matrix but also included were the C−H stretching and CH_3 deformation regions in order to increase the robustness of the analysis. An SVD was performed on the raw data matrix, and the resulting singular values indicated that only two physically real basis spectra are needed to account for 99.996% of the variance in the spectra. These physically real basis spectra are hypothesized to be the spectrum of self-associated ACN and the coadded spectra of the free ClO_4^- anion, the TEA^+ cation, and the ACN molecules influenced by ClO_4^-. Therefore, the following mathematical model was used to generate the matrix **P** that
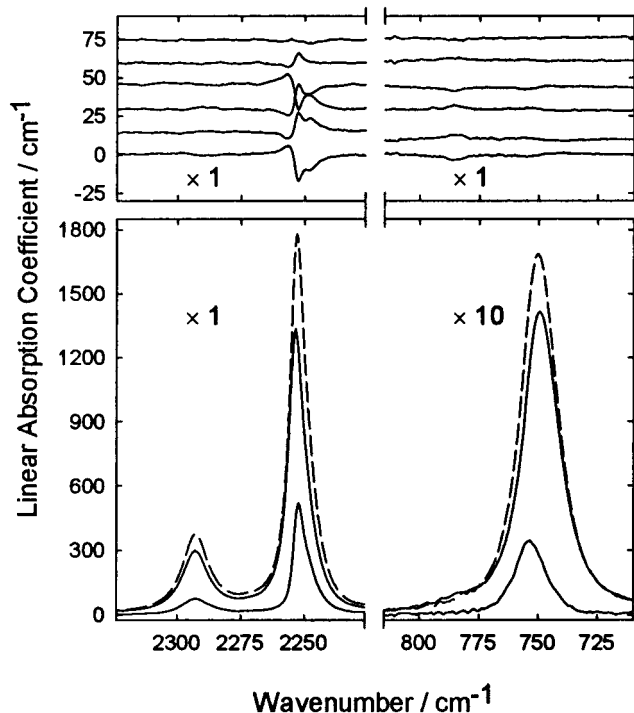
Figure 6. Multiple-dimensional curve fit of the ACN ν_2 and $2\nu_8$ spectral regions of TEAP–ACN spectra based the model encompassed by eq 1 and eq 2 in the text and using a number of solvent molecules influenced by ClO_4^- equal to 4. (top) The residuals shown (offset for clarity) are from the curve fits of 0.000 (pure ACN), 0.204, 0.365, 0.507, 0.621, and 0.680 M TEAP–ACN solution spectra (from bottom to top). (bottom) The curve fit of the 0.680 M TEAP–ACN solution spectrum. The measured spectrum is indicated with a dashed line.

accounts for the contribution of each physically real basis spectrum to each of the raw data spectra:

$$P_{1j} = \frac{c_{ACNj} - nc_{ej}}{c_{ACNm} - nc_{em}} \tag{1}$$

$$P_{2j} = \frac{c_{ej}}{c_{em}} \tag{2}$$

In the above equations, the subscript j indicates the jth column of **P**, n is the number of solvent molecules influenced by ClO_4^-, c_{ACNj} and c_{ej} are the concentrations of ACN and the electrolyte, respectively, in the jth solution, and the subscript m indicates that the concentration used was of the solution with the highest TEAP concentration. Equation 1 models the integrated absorbance of the self-associated ACN bands with respect to the value in the spectrum of the solution with the highest TEAP concentration. Equation 2 models the integrated absorbance of the bands of free ClO_4^-, TEA^+, and ClO_4^--associated ACN relative to the value in the spectrum of the solution with the highest concentrations of these species. With the use of this model, the computed physically real basis spectra are those spectra hypothesized above, but at the highest electrolyte concentration.

The number of solvent molecules influenced by ClO_4^- cannot be an unknown parameter in the model described above, since n is linear with respect to the raw data matrix **A** and cannot be separated from the global molar absorption coefficient of the spectrum of free ClO_4^- anion, TEA^+, and ClO_4^--associated ACN. However, n can be a fixed parameter. Consequently, multiple-dimensional curve fits were performed for a range of possible values of n. Figure 6 shows the curve fit of the spectrum
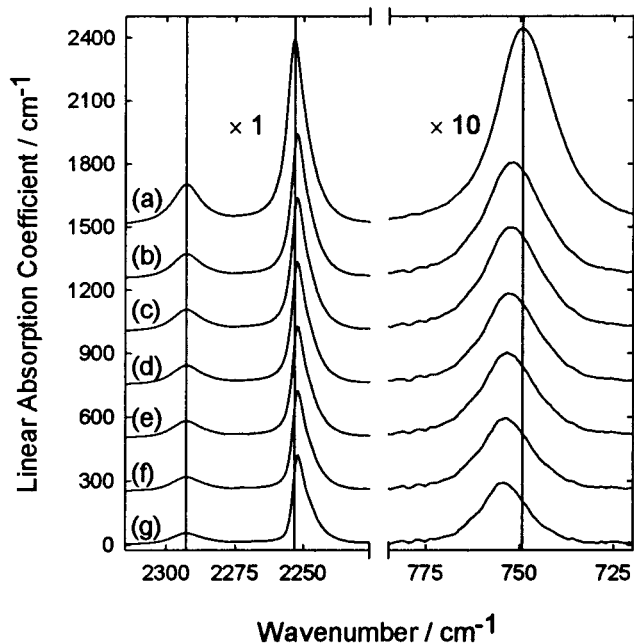

Figure 7. ACN ν_2 and $2\nu_8$ spectral regions of the physically real basis spectra accounting for ClO_4^--associated ACN, for possible values of the number of solvent molecules influenced by ClO_4^- equal to 8 (b), 7 (c), 6 (d), 5 (e), 4 (f), and 3 (g). These spectra result from the multiple-dimensional curve fit of the ACN ν_2 and $2\nu_8$ spectral regions of TEAP–ACN solutions based on the model encompassed by eqs 1 and 2 in the text. The spectrum of pure ACN is shown for comparison in (a). The spectra are offset for clarity.

of the solution with the highest concentration of TEAP, assuming that four solvent molecules are influenced by ClO_4^-. Also shown are the residuals from the curve fits of all six spectra used in the raw data matrix **A**. The residual of the curve fit of the 0.507 M TEAP solution accounts for only 0.63% of the integrated linear absorption coefficient of the measured spectrum, based on the spectral regions shown in Figure 6. It is notable that the physically real basis spectrum that accounts for self-associated ACN is identical to that of pure acetonitrile. Results, such as those shown in Figure 6, were obtained for all reasonable values of n; hence, the actual number of solvent molecules influenced by ClO_4^- could not be determined. Figure 7 shows the physically real basis spectrum due to ACN influenced by ClO_4^- for each value of n investigated, and the spectrum of pure ACN is shown for comparison. With an increase in the value of n, the $2\nu_8$ band of ClO_4^--associated ACN shifts further to the blue and the maximum linear absorption coefficients of all the ClO_4^--associated ACN bands grow larger. It should be noted that in both Figures 6 and 7, the TEA^+ bands at 797 and 786 cm^{-1} have been subtracted away for clarity.

The results of the multiple-dimensional curve fits of the spectra of the TEAP–ACN solutions were analyzed further to investigate the difference between the molar absorption coefficients of the ν_2 bands of ClO_4^--associated and self-associated ACN. Using the physically real basis spectrum that accounts for ClO_4^--associated ACN, the integrated area of the ν_2 band of ClO_4^--associated ACN was calculated via a single-dimensional curve fit similar to that used above to fit the ν_2 region of pure ACN. Next, a molar absorption coefficient was calculated by dividing the integrated area of the ν_2 band by the product of the number of solvent molecules influenced by ClO_4^- and the highest concentration of TEAP. Finally, a molar absorption coefficient ratio was calculated by dividing the molar absorption coefficient of the ν_2 band of ClO_4^--associated ACN
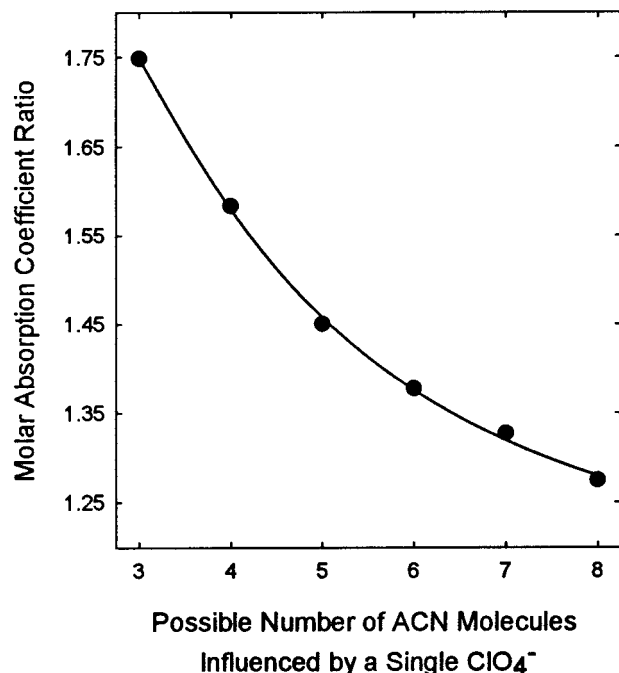
Ion−Solvent Interactions in Acetonitrile Solutions

J. Phys. Chem. A, Vol. 103, No. 19, 1999 **3615**

Figure 8. Ratio of the molar absorption coefficient of the ν_2 band of ClO_4^--associated ACN to the molar absorption coefficient of the ν_2 band of self-associated ACN versus possible values of the number of solvent molecules influenced by ClO_4^-.

by the molar absorption coefficient of the ν_2 band of self-associated ACN. This ratio has been plotted against possible values of n in Figure 8. It should be noted that if the number of solvent molecules influenced by ClO_4^- is equal to 4, then the molar absorption coefficient of the ν_2 band of ClO_4^--associated ACN is more than 50% larger than the molar absorption coefficient of the ν_2 band of self-associated ACN. In fact, at any reasonable value of n, the molar absorption coefficient of the ν_2 band of ClO_4^--associated ACN is substantially larger. Failure to discriminate between the ν_2 bands of self-associated and ClO_4^--associated ACN would lead to a substantial error in a calculated cation solvation number. This observation helps to explain the unusually low value of the average cation solvation numbers of Li^+ and Na^+ obtained via the single-dimensional fitting analyses described above.

Multiple-dimensional curve fits were also performed on the spectra of $LiClO_4-$ and $NaClO_4-ACN$ solutions, using the same spectral regions employed in the curve fits of the TEAP−ACN solution spectra shown above. The singular values resulting from an SVD of these spectra indicated that only two physically real basis spectra are needed to account for 99.992% and 99.994% of the variance in the $LiClO_4$ and $NaClO_4-ACN$ solution spectra, respectively. One would assume that if the vibrational bands of cation and ClO_4^--associated ACN were due to only ACN molecules associated with free ions, then the linear absorption coefficients of these bands would depend on the extent of ion pairing. However, an unexpected result is obtained if the model encompassed by eq 1 and eq 2 is used in the curve fit; in this case, the integer n must be interpreted as the sum of the number of solvent molecules influenced by both ClO_4^- and the cation. This model assumes that the linear absorption coefficients of the cation and ClO_4^--associated ACN bands, as well as the linear absorption coefficients of the self-associated ACN bands, depend only on the total electrolyte concentration and not on the extent of ion pairing. We point out that the quality of the curve fit using this model for the $LiClO_4-ACN$ solution spectra is unprecedented, as shown in
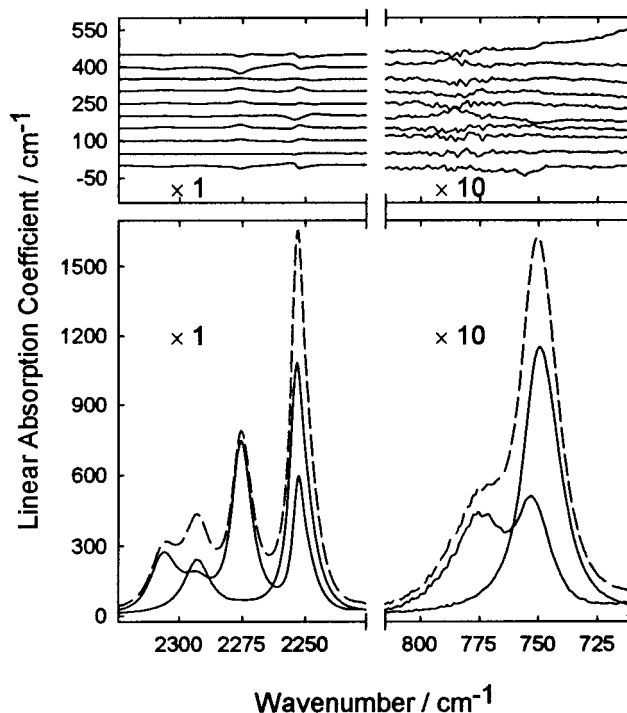

Wavenumber / cm⁻¹

Figure 9. Multiple-dimensional curve fit of the ACN ν_2 and $2\nu_8$ spectral regions of $LiClO_4-ACN$ solutions based the model encompassed by eqs 1 and 2 in the text and using a value of the total number of solvent molecules influence by both ClO_4^- and the Li^+ cation of 8. (top) Residuals (offset for clarity) are shown for the curve fits of the spectra shown in Figure 1. The bottom-most residual is from the curve fit of the pure ACN spectrum, and each successive residual is from the curve fit of the spectrum of greater $LiClO_4$ concentration (concentrations given in Figure 1). (bottom) The curve fit of the 0.887 M $LiClO_4-$ ACN solution spectrum. The measured spectrum is indicated with a dashed line.

Figure 9 for a possible value of n equal to 8. The residual of the curve fit of the 0.920 M $LiClO_4$ solution accounts for less than 1.4% of the integrated linear absorption coefficient of the measured spectrum, based on the spectral regions shown in Figure 9. Similar results are obtained from the multiple-dimensional curve fit of the $NaClO_4-ACN$ solution spectra.

Figure 10 shows the physically real basis spectrum that accounts for the ν_2 and $2\nu_8$ spectral regions of Li^+ and ClO_4^--associated ACN for each value of n investigated. The spectrum of pure ACN is also shown for comparison. Clearly evident is the slight red shift of the ν_2 band of ClO_4^--associated ACN, as well as the increasing blue shift of the $2\nu_8$ band of ClO_4^--associated ACN, with decreased value of n. These trends are identical to those seen in Figure 7 for the multiple-dimensional curve fits of the spectra of the TEAP−ACN solutions.

The dependence of the self-associated, the cation solvating, and the ClO_4^--associated ACN bands on electrolyte concentration, rather than on the extent of ion pairing, is most readily explained by assuming that the fraction of ion pairs, θ, is fairly constant over the concentration range studied. However, analysis of the vibrational bands of free and ion-paired ClO_4- shows that θ does vary with electrolyte concentration for both the $LiClO_4-$ and $NaClO_4-ACN$ solutions examined,[44] although the variation in θ may not be substantial enough to hinder a successful multiple-dimensional curve fit based on the model comprised by eqs 1 and 2.

An additional rationalization for the dependence of the bands of cation-solvating ACN on electrolyte concentration could be made by assuming that there is only one type of ion pair, that
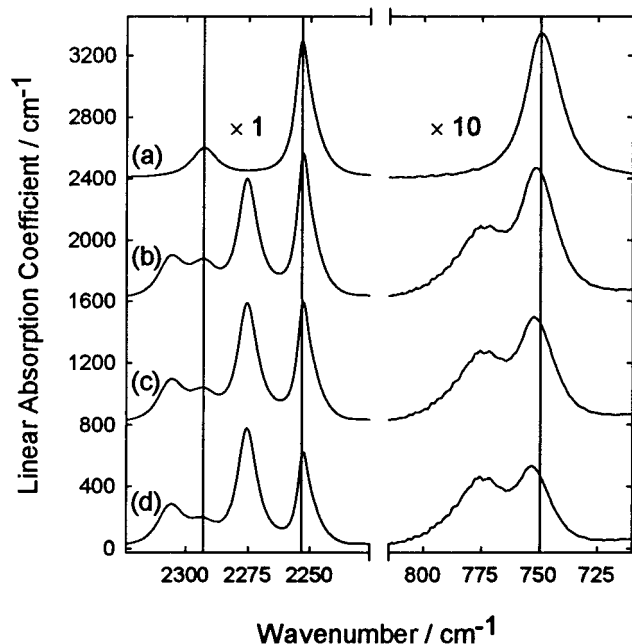
Figure 10. ACN ν_2 and $2\nu_8$ spectral regions of the physically real basis spectra accounting for ClO_4^--associated and Li^+-solvating ACN, for possible values of the total number of solvent molecules influence by ClO_4^- and solvating the Li^+ cation of 12 (b), 10 (c), and 8 (d). The spectra result from the multiple-dimensional curve fit of the ACN ν_2 and $2\nu_8$ spectral regions of $LiClO_4$−ACN solutions based the model encompassed by eqs 1 and 2 in the text. The spectrum of pure ACN is shown for comparison in (a). The spectra are offset for clarity.

this ion pair is solvated, and that the cation-solvating ACN bands are the coaddition of both free and ion-paired cation-solvating ACN bands. Under these circumstances, one could write

$$A_T = A_{M^+} + A_{IP} \tag{3}$$

$$A_T = \epsilon_{M^+} c_{M^+} + \epsilon_{IP} c_{IP} \tag{4}$$

where A_T is the total integrated linear absorption coefficient of the cation-solvating bands; A_{IP} and A_{M^+} are the integrated linear absorption coefficients of the ion-paired and free cation-solvating bands, respectively; ϵ_{IP} and ϵ_{M^+} are the molar absorption coefficients of the ion-paired and free cation-solvating bands, respectively; and c_{IP} and c_{M^+} are the concentrations of the ion pair and the free cation. Furthermore, if θ is the aforementioned fraction of ion pairs and n_{IP} and n_{M^+} are the solvation numbers of the ion pair and the free cation, respectively, then

$$A_{Total} = \epsilon_{M^+} n_{M^+} (1-\theta) c_e + \epsilon_{IP} n_{IP} \theta c_e \tag{5}$$

and

$$A_{Total} = (\epsilon_{IP} n_{IP} - \epsilon_{M^+} n_{M^+}) \theta c_e + \epsilon_{M^+} n_{M^+} c_e \tag{6}$$

It follows from eq 6 that the dependence of a cation-solvating ACN band on electrolyte concentration would be observed either if θ were nearly constant over the electrolyte concentration range studied or if $\epsilon_{IP} n_{IP} \cong \epsilon_{M^+} n_{M^+}$. Since semiempirical quantum mechanical calculations by Perelygin[41,42] show that the difference between the charge distribution of an ACN molecule solvating a free cation and the charge distribution of an ACN molecule solvating a cation in a solvent-separated ion pair is not significant when compared with the difference between the charge distribution of an ACN molecule solvating a free cation and the charge distribution of a free ACN molecule, it may be

possible that $\epsilon_{IP} n_{IP} \cong \epsilon_{M^+} n_{M^+}$, as long as the formation of an ion pair does not significantly displace ACN from the cation's solvation shell. This result of Perelygin's computations also supports the assumption that both free and ion-paired cation-solvating ACN bands have the same wavenumber positions. However, assuming that $\epsilon_{IP} n_{IP} \cong \epsilon_{M^+} n_{M^+}$ does not help to explain why the linear absorption coefficient of the vibrational bands of self-associated and ClO_4^--associated ACN vary linearly with electrolyte concentration.

Conclusions

In the present study, it has been shown that the interaction of ClO_4^- anions with ACN significantly alters the spectrum of the solvent in its ν_2 and $2\nu_8$ spectral regions. This finding contradicts the assumption made in previous vibrational spectroscopic analyses of alkali and alkaline earth metal perchlorate−ACN solutions that the ν_2 band of ClO_4^--associated ACN is indistinguishable from the ν_2 band of self-associated ACN. The analyses performed in the previous studies relied on this assumption in order to calculate cation solvation numbers.[7,12−15] Because the molar absorption coefficient of the ν_2 band of ClO_4^--associated ACN is substantially larger than that of self-associated ACN, the previously reported cation solvation numbers are believed to be unreliable.

It also has been demonstrated in this study that the integrated linear absorption coefficients of the cation solvating, ClO_4^--associated, and self-associated ACN bands depend on total electrolyte concentration, rather than on the extent of ion pairing. It has been proposed that this dependence may be due to a nearly constant value of the fraction of ion pairs over the concentration range of electrolyte studied or due in part to the approximate equality $\epsilon_{IP} n_{IP} \cong \epsilon_{M^+} n_{M^+}$. Most likely, a combination of these explanations accounts for this phenomenon.

The powerful methods of curve fitting used in the present study have allowed the most careful and detailed solvation analysis of the vibrational spectra of the $LiClO_4$, $NaClO_4$, and TEAP systems in ACN to date. As a result, a greater understanding of the role of the anion and its effects on the vibrational spectrum of the solvent has been achieved. Some aspects of ion solvation in these systems, such as the solvation number of the cation, may remain undetermined by vibrational spectroscopy alone. However, when combined with other powerful and complimentary techniques such as nuclear magnetic resonance (NMR) spectroscopy, X-ray and neutron diffraction, and extended X-ray absorption fine structure (EXAFS) spectroscopy, the details of electrolyte solvation can be elucidated.[45]

References and Notes

(1) Gardiner, D. J. Vibrational Spectra of Non-Aqueous Solutions. In *Advances in Infared and Raman Spectroscopy*; Clark, R. J. H., Hester, R. E., Eds.; Heyden: London, 1976; Vol. 3, p 167.

(2) Irish, D. E.; Brooker, M. H. Raman and Infrared Studies of Electrolytes. In *Advances in Infrared and Raman Spectroscopy*; Clark, R. J. H., Hester, R. E., Eds.; Heyden: London, 1976; Vol. 2, p 212.

(3) Perelygin, I. S. Infrared spectra and solvation of ions. In *Ionic Solvation*; Krestov, G. A., Ed.; Ellis Horwood: New York, 1994; p 100.

(4) Perelygin, I. S. *Opt. Spectrosc.* **1962**, *13*, 198.

Ion−Solvent Interactions in Acetonitrile Solutions

J. Phys. Chem. A, Vol. 103, No. 19, 1999 **3617**

(5) Kecki, Z.; Witanowski, J. *Rocz. Chem.* **1964**, *38*, 691.

(6) Kecki, Z.; Wojtczak, J. *Rocz. Chem.* **1970**, *44*, 847.

(7) Perelygin, I. S.; Klimchuk, M. A. *Russ. J. Phys. Chem.* **1973**, *47*, 1138.

(8) Perelygin, I. S.; Klimchuk, M. A. *Russ. J. Phys. Chem.* **1974**, *48*, 363.

(9) Chang, T. G.; Irish, D. E. *J. Solution Chem.* **1974**, *3*, 161.

(10) Borisova, V. B.; Markelov, V. V.; Akopyan, S. K.; Shevyakov, A. M.; Bakhshiev, N. G. *Russ. J Phys. Chem.* **1979**, *53*, 215.

(11) Sastry, M. I. S.; Singh, S. *Curr. Sci.* **1986**, *55*, 1157.

(12) Fawcett, W. R.; Liu, G. *J. Phys. Chem.* **1992**, *96*, 4231.

(13) Fawcett, W. R.; Liu, G.; Faguy, P. W.; Foss, C. A.; Motheo, A. J. *J. Chem. Soc., Faraday Trans.* **1993**, *85*, 811.

(14) Fawcett, W. R.; Liu, G.; Kloss, A. A. *J. Chem. Soc., Faraday Trans.* **1994**, *90*, 2697.

(15) Barthel, J.; Deser, R. *J. Solution Chem.* **1994**, *23*, 1133.

(16) Barthel, J. *J. Mol. Liq.* **1995**, *65/66*, 177.

(17) Radnai, T.; Itoh, S.; Ohtaki, H. *Bull. Chem. Soc. Jpn.* **1988**, *61*, 3845.

(18) Radnai, T.; Jedlovszky, P. *J. Phys. Chem.* **1994**, *98*, 5994.

(19) Radnai, T.; Bakó, I.; Jedlovszky, P.; Pálinkás, G. *Mol. Simul.* **1996**, *16*, 345.

(20) Izdebska, B.; Kecki, Z. *Rocz. Chem.* **1978**, *52*, 1531.

(21) Pominov, I. S.; Serzhantova, V. N. *Zh. Prikl. Spektrosk.* **1970**, *12*, 1071.

(22) Bertie, J. E. *Appl. Spectrosc.* **1985**, *39*, 392.

(23) Bertie, J. E.; Zhang, S. L.; Manji, R. *Appl. Spectrosc.* **1992**, *46*, 1660.

(24) Belali, R.; Vigoureux, J.-M.; Morvan, J. *J. Opt. Soc. Am. B* **1995**, *12*, 2377.

(25) Loring, J. S. *LinkFit*; 1996−1999.

(26) Loring, J. S. *SVD Spectral Analysis Tool*; 1997−1999.

(27) Loring, J. S. *Spectral Conversion Tool*; 1998−1999.

(28) Sperline, R. P.; Muralidharan, S.; Freiser, H. *Appl. Spectrosc.* **1986**, *40*, 1019.

(29) Bertie, J. E.; Zhang, S. L.; Jones, R. N.; Apelbat, Y.; Keefe, C. D. *Appl. Spectrosc.* **1995**, *49*, 1821.

(30) Bertie, J. E.; Lan, Z. *J. Chem. Phys. B* **1996**, *101*, 4111.

(31) Hug, S. J.; Sulzberger, B. *Langmuir* **1994**, *10*, 3587.

(32) Griffiths, J. E. *J. Chem. Phys.* **1973**, *59*, 751.

(33) Loewenschuss, A.; Yellin, N. *Spectrochim. Acta* **1975**, *31A*, 207.

(34) Loewenschuss, A.; Yellin, N. *Spectrochim. Acta* **1976**, *32A*, 1249.

(35) Fawcett, W. R.; Liu, G.; Kessler, T. E. *J. Phys. Chem.* **1993**, *97*, 9293.

(36) Fini, G.; Mirone, P. *Spectrochim. Acta* **1976**, *32A*, 625.

(37) Hashimoto, S.; Ohba, T.; Ikawa, S.-i. *Chem. Phys.* **1989**, *138*, 63.

(38) Suzuki, I.; Nakagawa, J.; Fujiyama, T. *Spectrochim. Acta* **1977**, *33A*, 689.

(39) Venkateswarlu, P. *J. Chem. Phys.* **1951**, *19*, 293.

(40) Gutmann, V. *The Donor−Acceptor Approach to Molecular Interactions*; Plenum: New York, 1978.

(41) Perelygin, I. S.; Shatokhin, S. A.; Karpasas, M. M. *Russ. J. Phys. Chem.* **1993**, *67*, 1990.

(42) Perelygin, I. S.; Shatokhin, S. A. *J. Mol. Struct.* **1998**, *440*, 89.

(43) Mathieu, D.; Defranceschi, M.; Lécayon, G.; Delhalle, J. *C. R. Acad. Sci. Paris* **1992**, *315*, 1181.

(44) Loring, J. S.; Fawcett, W. R. Unpublished results, 1995.

(45) *The Chemical Physics of Solvation*; Dogonadze, R. R., Kalman, E., Kornyshev, A. A., Ulstrup, J., Eds.; Elsevier: New York, 1986; Vol. 38, p 559.